mTORC2 contributes to murine lupus

Xian Zhou[1], Haiyu Qi[1,2], Yanfeng Li[1], Xingxing Zhu[1], Shreyasee Amin[1], Mariam Alexander[3], Catherine Diadhiou[4,5], Anne Davidson[4,5], Hu Zeng[1,6]

[1]Division of Rheumatology, Department of Medicine, Mayo Clinic Rochester, MN 55905, USA

[2]Department of Rheumatology, Beijing Friendship Hospital, Capital Medical University, Beijing, 100050, P. R. China

[3]Division of Laboratory Medicine and Pathology, Mayo Clinic Rochester, MN 55905, USA

[4]Institute of Molecular Medicine, Feinstein Institutes for Medical Research, Manhasset, NY 11030, USA

[5]Donald and Barbara Zucker School of Medicine at Hofstra/Northwell, Manhasset, NY 11030, USA

[6]Department of Immunology, Mayo Clinic Rochester, MN 55905, USA

Address correspondence and reprint request to Dr. Hu Zeng, Division of Rheumatology, Department of Medicine, Mayo Clinic Rochester, Guggenheim Building 3-42, 200 First ST SW, Rochester, MN, 55902, USA. E-mail address: zeng.hu1@mayo.edu.

Abbreviations used in this article: Tfh, follicular helper T cells; Treg, regulatory T cells; SLE, systemic lupus erythematosus; mTOR, mechanistic target of rapamycin; IFN, interferon; GC, germinal center; EF, extrafollicular; Tfr, follicular regulatory T cells; ICOS, inducible T-cell costimulatory.

ABSTRACT

The development of systemic lupus erythematosus (SLE) is associated with overactivation of the type I interferon (IFN) pathway, lymphopenia, and increased follicular helper T (Tfh) cell differentiation. However, the cellular and molecular mechanisms of action of type I IFN in SLE remains incompletely understood. Here we show that type I IFN activates the mechanistic target of rapamycin complex 2 (mTORC2) in T cells to promote T cell lymphopenia. mTORC2 also promotes Tfh differentiation and disrupts Treg homeostasis. Inactivation of mTORC2 greatly ameliorated the immunopathology in a lupus-prone mouse model, associated with reduced Tfh differentiation, normalization of Treg homeostasis and reduced T cell glucose metabolism. These data indicate that mTORC2 acts downstream of type I IFN and costimulatory receptor ICOS, to promote T cell lymphopenia and Tfh differentiation in murine lupus development, suggesting that inhibition of mTORC2 could limit lupus disease progression.

36 **INTRODUCTION**

37 Overactivation of the type I IFN pathway is a prominent feature of SLE, both in patients and
38 mouse models (1, 2). Therapeutical options blocking type I IFN, or its receptor have shown
39 clinical efficacy (3). Yet, the specific cellular and molecular mechanisms by which type I IFN
40 promotes SLE pathology remain incompletely understood. Recent studies using murine lupus
41 models have demonstrated that type I IFN signaling in $CD4^+$ T cells are required for
42 development of lupus pathology (4, 5). In addition, it is well established that type I IFN can
43 block T cell egress from lymph nodes and induce lymphopenia partly by upregulating the
44 expression of CD69 (6, 7), a marker that is also associated with lupus pathology (8, 9).
45 Moreover, elevated type I IFN activity is highly correlated with lymphopenia in SLE patients
46 (10). However, the type I IFN signaling pathway in $CD4^+$ T cells remains incompletely
47 understood and it is unclear how type I IFN overactivation may be linked to T cell lymphopenia
48 in lupus.

49

50 It is increasingly recognized that a loss of balance between effector and regulatory $CD4^+$ T
51 (Treg) cells is associated with the development of systemic lupus erythematosus (SLE) (11).
52 Increased differentiation of follicular helper T (Tfh) cells has been associated with SLE
53 development and severity in mouse models and human patients (12, 13). Germinal center (GC)
54 Tfh cells, distinguished by expression of the transcription factor BCL6, chemokine receptor
55 CXCR5, and immune checkpoint receptor PD-1, are a specialized effector T cell lineage that
56 stimulate B cells in GC to undergo affinity maturation and clonal expansion. The costimulatory
57 receptor ICOS delivers critical signals for Tfh differentiation (14). In addition, a special subset of
58 Tfh cells with low expression of CXCR5 and P-selectin ligand, PSGL-1, are localized in

59 extrafollicular (EF) to promote generation of plasmablasts, which produce antibodies with
60 modest affinity (15-17). Both GC and EF responses may contribute to SLE development (18). In
61 contrast, impaired Treg function is observed in SLE patients (19), including a reduced expression
62 of CD25 (20), the IL-2 receptor alpha chain that is essential for Treg homeostasis and function.
63 However, what drives the imbalance between Tfh and Tregs in lupus is not well understood.
64
65 Mechanistic target of rapamycin (mTOR) is a central metabolic pathway, which consists of two
66 complexes, mTORC1 and mTORC2, with scaffolding molecules RAPTOR (encoded by *RPTOR*)
67 and RICTOR (encoded by *RICTOR*) as their defining components, respectively (21). mTORC1
68 is critical for naïve T cell quiescence exit and proliferation, and all effector T cell differentiation
69 (22). In contrast, mTORC2 is essential for Tfh differentiation, but dispensable for T cell
70 activation and modestly contributes to other effector T cell lineages (22). Ligation of ICOS
71 activates mTORC2, which in turn promotes glucose metabolism in Tfh cells (23). In terms of
72 Tregs, mTORC1 maintains natural or thymic derived Treg (nTreg, or tTreg) functional
73 competency (24-27). Overactivation mTORC2 reduces CD25 expression on Tregs, increases
74 Treg frequency in peripheral lymphoid organs, and impairs Treg suppressive function and
75 stability, especially their ability to suppress Tfh cells, which leads to systemic autoimmune
76 disease with lupus characteristics (28, 29). Inhibition of mTORC2 in Tregs can partly restore
77 tolerance in the absence of mTORC1 (24), or FOXP3 (30). Therefore, mTORC2 signaling
78 controls the balance between Tfh and Treg by promoting the former and suppressing the latter.
79 These fundamental discoveries suggest that targeting mTORC2 in T cells may benefit lupus
80 disease, while largely spare Th1 and Th17 lineages compared to targeting mTORC1, hence with
81 relatively reduced immunosuppressive side effects.

82

83 Several studies have examined the contribution of mTORC1 to SLE development (31). How
84 mTORC2 contributes to SLE pathology has been much less understood. A modest reduction of
85 mTORC2 in lupus patient T cells was initially suggested (32), but a later study showed an
86 increased mTORC2 activity in activated Tregs from lupus patients (33). Here, we demonstrate
87 that type I IFN can sustain mTORC2 activation and promotes CD69 expression, which
88 suppresses T cell egress and leads to lymphopenia, partly in an mTORC2 dependent manner. We
89 further tested the hypothesis that genetic targeting mTORC2 in T cells can benefit lupus in a
90 classic murine lupus model, C57BL/6-*Fas*^{Lpr} (Lpr) mice. We show that Lpr T cells have an
91 elevated base line activity of mTORC2. Loss of *Rictor* specifically in T cells significantly
92 improves immunopathology in Lpr mice, including T cell lymphopenia and generation of
93 autoantibodies, which is associated with normalization of the balance between Tfh cells and
94 Tregs, without significant changes in Th1 or Th17 lineages. Our data suggest that mTORC2 in T
95 cells contributes to the immunopathogenesis of lupus, and thus it may constitute a promising
96 target for lupus treatment.

97

98 **RESULTS**

99 **mTORC2 functions downstream of type I IFN to promote CD69 expression and suppress T**
100 **cell egress**

101 Lpr mice recapitulate many of the immunological phenotypes in human disease (34). We tested
102 whether mTORC2 activity is altered in T cells from Lpr mice. Immunoblot analysis showed that
103 $CD4^+$ T cells from Lpr mice had elevated phosphorylation of AKT at Serine 473 (p-AKT_{473}), a
104 direct target of mTORC2, indicating overactivation of mTORC2 in Lpr T cells at baseline (Fig.

105 1A). Previous studies have identified that type I IFN contributes to the lupus phenotypes in Lpr
106 mice (35, 36). We found that addition of IFNα significantly enhanced anti-CD3/anti-CD28
107 induced p-AKT_{473} at 6 h stimulation, which was completely dependent on RICTOR (Fig. 1B).
108 IFNα alone could also induced p-AKT_{473}, but the combination of anti-CD3/anti-CD28 and IFNα
109 appeared to be the most potent activators of RICTOR dependent p-AKT_{473} (Fig. 1C). Thus,
110 IFNα, in synergy with anti-CD3/anti-CD28, promoted p-AKT_{473} in a RICTOR dependent
111 manner. RICTOR deficiency did not markedly affect canonical IFNα–STAT1 signaling, but
112 modestly attenuated STAT2 phosphorylation (Fig. 1B and Supplementary Fig. 1A). While
113 RICTOR deficiency did not affect mTORC1 activation (Supplementary Fig. 1A). Type I IFN is
114 known to suppress lymphocyte egress from lymph nodes to blood, partly through induction of
115 CD69 expression (6, 7). Indeed, administering poly(I:C), which stimulates type I IFN
116 production, induced potent CD69 expression on blood $CD4^+$ T cell (Fig. 1D), and induced $CD4^+$
117 T cell lymphopenia (Fig. 1E). Both phenotypes were significantly reversed in $CD4^+$ T cells from
118 $CD4^{Cre}$*Rictor*$^{fl/fl}$ mice. Such phenotype was not observed in $CD19^+$ B cells, in which RICTOR
119 was intact (Supplemental Fig. 1B), indicating that type I IFN promotes $CD4^+$ T cell lymphopenia
120 partly through T cell intrinsic mTORC2. Consistent with these observations, Lpr $CD4^+$ T cells
121 had increased CD69 level, which was completely restored in C57BL/6.*Fas*^{Lpr}*Cd4*^{Cre}*Rictor*$^{fl/fl}$
122 (Lpr.*Rictor*$^{-/-}$) mice in both lymph nodes and blood (Fig. 1F, Supplemental Fig. 1C).
123 Importantly, the severe $CD4^+$ T cell lymphopenia phenotype in Lpr mice was also partially
124 reversed by RICTOR deficiency (Fig. 1G, Supplemental Fig. 1D). Therefore, $CD4^+$ T cells from
125 lupus prone mouse model exhibited increased mTORC2 activity. Type I IFN activates mTORC2
126 to induce CD69 expression on $CD4^+$ T cells and block $CD4^+$ T cell egress into blood. RICTOR
127 deficiency partially restores $CD4^+$ T cell lymphopenia in Lpr mice.

128

129 **Loss of mTORC2 in CD4$^+$ T cells improves immunopathology in experimental murine**

130 **lupus**

131 Based on above results, we predicted that *Rictor* deletion in T cells would ameliorate lupus

132 pathology in Lpr mice. RICTOR deficiency in T cells alone does not significantly impact

133 immune cell homeostasis and overall mouse health (24, 37, 38), therefore we focused on the

134 comparison among B6, Lpr mice and Lpr.*Rictor*$^{-/-}$ mice. *Fas*^{Lpr} mutation drives dramatic

135 lymphoid hyperplasia, including splenomegaly and lymphadenopathy. We observed that deletion

136 of *Rictor* in T cells significantly rescued the splenomegaly and lymphadenopathy phenotypes, in

137 terms of both organ size and total cellularity (Fig. 2A, B). Consistent with these findings, Lpr

138 mice had highly increased total IgM and IgG, and isotypes IgG2b and IgG3 immunoglobulin

139 levels (Fig. 2C) and increased anti-ssDNA and anti-chromatin autoantibodies (Fig. 2D), all of

140 which were significantly reduced in Lpr.*Rictor*$^{-/-}$ mice. Furthermore, we examined IgG and

141 complement deposition in kidneys, which reflects lupus disease severity. Lpr mice on B6

142 background have very mild kidney pathology compared to those on MRL/MpJ background (39).

143 Consistent with this observation, we oberved a modest increase of IgG and complement C3

144 deposition in kidneys from Lpr mice. Deletion of Rictor significantly reduced IgG deposition.

145 While there was a trend of reduced C3 deposition in Lpr.*Rictor*$^{-/-}$ kidney, it did not reach

146 statistical significance (Supplemental Fig. 2A). Thus, inactivation of mTORC2 in T cells

147 substantially attenuates lymphoid hyperplasia, antibody secretion, and renal immune complex

148 deposition in a lupus prone mouse model.

149 Consistent with the attenuated lymphoid hyperplasia in Lpr.*Rictor*$^{-/-}$ mice, the accumulation of

150 the aberrant B220$^+$TCRβ$^+$ cells in Lpr mice was nearly completely reversed in Lpr.*Rictor*$^{-/-}$ mice

151 (Fig. 2E). Although Lpr.*Rictor*$^{-/-}$ mice had a significant increase of B220^{+}TCRβ^{-} B cell
152 percentage, the absolute number of this population highly reduced in Lpr.*Rictor*$^{-/-}$ mice
153 compared to Lpr mice (Fig. 2E). B220^{-}TCRβ^{+} T cell percentages were highly reduced in both
154 Lpr and Lpr.*Rictor*$^{-/-}$ mice, but Lpr mice had substantial increase of B220^{-}TCRβ^{+} T cell number
155 likely due to the lymphoid hyperplasia, which was also reversed in Lpr.*Rictor*$^{-/-}$ mice (Fig. 2E).
156 Finally, the accumulation of TCRβ^{+}CD4^{-}CD8^{-} DN T cells was almost completed restored by
157 *Rictor* deletion (Fig. 2F). Therefore, the inactivation of mTORC2 in T cells significantly reverses
158 the abnormal accumulation of T and B cells and restores immune homeostasis in peripheral
159 lymphoid organs of Lpr mice.
160
161 **mTORC2 in T cells promotes B cell hyper-activation**
162 Reflecting the enhanced antibody levels, immunofluorescence staining revealed a dramatic
163 increase of peanut agglutinin (PNA) staining in Lpr mice. The pattern of the PNA staining was
164 variable. Some are dense aggregations similar to defined GC formation, but others are more
165 diffused without defined boundaries (Fig. 3A). T cell distribution was also disorganized in Lpr
166 lymphoid tissues. Both the increased PNA staining and disorganized T cell distribution were
167 greatly restored by RICTOR deficiency (Fig. 3A). Flow cytometry analysis confirmed these
168 observations. B cells from Lpr mice had highly increased expression of germinal center B cell
169 marker GL-7, and significant loss of IgD expression, indicating increased B cell activation and
170 class switch (Fig. 3B). Consistent with this notion, Lpr B cells had greatly increased IgG1
171 expression (Supplemental Fig. 3A). A large proportion of Lpr B cells lost expression of CD38, a
172 NADase with strong immunosuppressive capacity (40), and the loss of which is another
173 characteristic of germinal center B cells (Supplemental Fig. 3A). Because plasmablasts

174 contribute to extrafollicular response, we stained CD138, a marker of plasmablasts. The results
175 showed a markedly increase of CD138 expression in extrafollicular region of Lpr spleens, which
176 was reduced in Lpr.*Rictor*$^{-/-}$ mice (Fig. 3C). The RICTOR-dependent increase of extrafollicular
177 response in Lpr mice was confirmed with flow cytometry analysis. Lpr mice accumulated large
178 number of cells with modest expression of CD138, and B220^{lo}CD138^{hi} plasmablast/plasma cells,
179 while deletion of *Rictor* in T cells dramatically suppressed the generation of these populations
180 (Fig. 3D). Therefore, mTORC2 activity in T cells is a major contributor to B cell abnormality in
181 Lpr mice. mTORC2 in T cells is required for GC reaction in immunization and viral infection
182 models (23). B220^{lo}CD138^{+} plasmablasts typically form at EF location (41). We observed
183 significantly reduced plasmablast frequency in *OX40*^{Cre}*Rictor*$^{fl/fl}$ mice, in which *Rictor* was
184 deleted in activated T cells (23), compared to WT mice either following LCMV infection or
185 peptide immunization (Supplemental Fig. 3B, 3C). Thus, mTORC2 in T cells is required for GC
186 reaction and CD138^{+} plasmablast cell formation during foreign antigen challenges and
187 autoimmune response. Taking together, our data support a model in which inhibition of
188 mTORC2 in T cells simultaneously attenuates B cell activation through both GC and EF
189 pathways in Lpr mice, and hence suppresses lupus development.
190

191 **Increased Tfh differentiation in Lpr mice is dependent on mTORC2**

192 Tfh is key for GC formation. Indeed, we observed many T cells in GC of Lpr mice from
193 immunofluorescence staining, presumably Tfh cells (Fig. 3A). This was confirmed by flow
194 cytometry data, which showed a strong increase of BCL6^{+}CXCR5^{hi} GC Tfh and BCL6^{-}CXCR5^{+}
195 pre-Tfh cells in Lpr.*Rictor*$^{-/-}$ mice, that was significantly dependent on RICTOR expression (Fig.
196 4A and Supplemental Fig. 4A for gating strategy). A RICTOR-dependent CXCR5 expression

197 was also found on TCRβ^{+}CD4^{-}CD8^{-} DN T cells (data not shown). Similar observations were
198 found when using other conventional Tfh markers, PD-1 and CXCR5 (Supplemental Fig. 4B).
199 RICTOR deficiency also reduced PSGL-1^{-}CXCR5^{-} EF Tfh cell frequency (Fig. 4B), consistent
200 with the reduction of plasmablast/plasma cells. These results indicated a critical requirement of
201 mTORC2 signaling for autoreactive GC and EF Tfh differentiation in Lpr lupus model. Similar
202 rescue effects were observed at different ages (at 3 and 9 months, data not shown). Like SLE
203 patients (13), Lpr mice had highly increased ICOS expression, both on CXCR5^{+} and CXCR5^{-} T
204 cells. Interestingly, deletion of *Rictor* failed to restore ICOS expression, indicating that the
205 reduced Tfh differentiation in Lpr.*Rictor*$^{-/-}$ mice is not a consequence of reduced ICOS
206 expression (Fig. 4C).
207 Treg cells are key to maintain immune tolerance and prevent autoimmunity. Counterintuitively,
208 in an inflammatory condition, Treg percentage sometimes increases. But those Tregs are often
209 dysfunctional (24, 28). We found that Lpr mice had variable Treg perturbations dependent on
210 anatomic location: while Treg percentages increased the most in spleens and modestly in
211 peripheral lymph nodes (pLN), they trended lower in the gut mucosal site relative to WT B6
212 mice (Fig. 4D), in a manner consistent with the graded mTORC2 activity, gradually increasing
213 from spleen to pLN, and to gut mucosal site (23). In all cases, deletion of *Rictor* significantly
214 restored the Treg homeostasis in Lpr mice (Fig. 4D). The magnitude of changes of Treg
215 frequencies in Lpr mice was much smaller than that of Tfh cells, thus the ratio between Tfh and
216 Treg was drastically increased in Lpr mice, suggesting an imbalance between Tfh and Tregs in
217 Lpr mice. Such imbalance was significantly restored by mTORC2 deficiency (Fig. 4E).
218 FOXP3^{+}CXCR5^{+} follicular regulatory T (Tfr) cells are specialized to suppress Tfh cells and GC
219 formation (42). RICTOR deficiency alone does not impact Tfr differentiation (23). Lpr mice had

220 highly increased ratio between Tfh and Tfr cells, which was partly restored in Lpr.*Rictor*$^{-/-}$ mice
221 (Fig. 4E). However, Lpr mice also had significantly increased frequency of FOXP3^{+}CXCR5^{+} Tfr
222 cells compared to B6 control mice, which was also reversed by *Rictor* deletion (Supplemental
223 Fig. 4C). Therefore, the data indicate that RICTOR deficiency impacts Tfh/Tfr ratio primarily by
224 reducing Tfh, not increasing Tfr. Furthermore, consistent with increased mTORC2 activity and
225 reduced CD25 expression in Tregs from lupus patients, Tregs from Lpr mice exhibited reduced
226 CD25 expression (Supplemental Fig. 4D) and reduced FOXP3 expression (Supplemental Fig.
227 4E), both of which were fully restored in Lpr.*Rictor*$^{-/-}$ mice.
228 Furthermore, we found that *Rictor* deficiency did not restore the increased IFNγ expression (Fig.
229 4F), or alter IL-2 and IL-17 expression in CD4^{+} T cells from Lpr mice (Fig. 4F, 4G), or change
230 the expression of lineage transcription factor Tbet and Rorγt (Supplemental Fig. 4F), consistent
231 with our hypothesis that mTORC2 inactivation preferentially affects Tfh differentiation, but not
232 other effector T cell lineages. These data also suggested that Tregs from Lpr.*Rictor*$^{-/-}$ mice were
233 not able to control the excessive cytokine production in Lpr CD4^{+} T cells, despite normalization
234 of their homeostasis. Finally, the restoration of T cell phenotypes in Lpr.*Rictor*$^{-/-}$ mice was likely
235 independent of cell proliferation, because CD4^{+} T cells from Lpr.*Rictor*$^{-/-}$ mice had similarly
236 increased Ki-67^{+} percentage at steady state as those from Lpr mice (Fig. 4H). Therefore, our data
237 showed that mTORC2 contributes to the increased GC and EF Tfh cells in Lpr mice,
238 independent of ICOS receptor expression and T cell proliferation.
239
240 **Inactivation of mTORC2 restores T cell glucose metabolism**
241 Recent studies indicate that lupus development is associated with dysregulation of T cell
242 immunometabolism (43). mTORC2 is known as one of the key regulators for cell metabolism.

243 We compared the basal respiration and glycolysis of T cells among B6, Lpr and Lpr.*Rictor*$^{-/-}$
244 mice at different ages under TCR signaling stimulation. Consistent with recent publications (44,
245 45), T cells from 2 months old Lpr mice had modestly increased basal respiration and glycolysis
246 (Fig. 5A, 5B). Strikingly, T cells from 3 and 9 months old Lpr mice had dramatically decreased
247 basal respiration and glycolysis, relative to B6 mice (Fig. 5A, 5B). The opposite metabolic
248 activities between 2 and 3 months old Lpr mice T cells were associated with drastic changes of
249 naive and effector T cell composition at different ages of Lpr mice during lupus development
250 (Supplemental Fig. 5A). Lpr.*Rictor*$^{-/-}$ mice had much lower levels of basal respiration and
251 glycolysis compared to B6 mice at all ages (Fig. 5A, 5B). The reduced metabolic activity in
252 primary culture of T cells from older Lpr and Lpr.*Rictor*$^{-/-}$ mice (compared to 2 months old
253 mice) was consistent with reduced T cell proliferation during primary culture (Supplemental Fig.
254 5B), and increased expression of senescence and anergy markers on Lpr CD4^{+} T cells at steady
255 state. None of these phenotypes were substantially affected by RICTOR deficiency
256 (Supplemental Fig. 5C). We have previously shown that mTORC2 functioned downstream of
257 ICOS receptor to promote Tfh differentiation, which could be modeled by restimulating
258 previously activated T cells with anti-CD3/anti-ICOS (23). Interestingly, Lpr T cells had greatly
259 enhanced proliferation during secondary activation with anti-CD3/anti-ICOS regardless of the
260 ages (Supplemental Fig. 5D, and data not shown). All these defects were not markedly affected
261 by RICTOR deficiency, again reaffirming that RICTOR deficiency did not significantly affect
262 the proliferation of Lpr T cells. Previous studies have demonstrated that mTORC2 promotes
263 TCR/ICOS mediated glucose metabolism during Tfh differentiation (23). Therefore, we
264 examined the T cell glycolysis after anti-CD3/anti-ICOS secondary stimulation. Lpr CD4^{+} T
265 cells exhibited a significant increase of compensatory glycolytic rate relative to B6 controls,

266 regardless of the ages. *Rictor* deletion substantially reduced both basal and compensatory
267 glycolytic rate in Lpr $CD4^+$ T cells (Fig. 5C). Therefore, mTORC2 contributes to the enhanced
268 glycolysis in Lpr T cells.
269
270 **DISCUSSION**
271 In this study, we made several key observations: 1) Type I IFN promotes mTORC2 activation in
272 $CD4^+$ T cells partly to drive CD69 expression and T cell lymphopenia; 2) T cells in Lpr mice
273 have elevated mTORC2 activity and mTORC2 inhibition through genetic deletion of RICTOR in
274 T cells can significantly ameliorate immunopathology of Lpr mice, including increased GC B
275 cells and extrafollicular B cells; 3) RICTOR deficiency restores Tfh and Treg balance in Lpr
276 mice, without significant alteration of T cell proliferation and Th1 and Th17 lineages; 4)
277 RICTOR deficiency reduces ICOS-mediated glycolysis in Lpr T cells. Thus, our study identifies
278 mTORC2 as a potential therapeutic target for lupus.
279
280 It has long been established that exuberant type I IFN activity contributes to lupus development.
281 Yet, the molecular mechanism through which type I IFN impact T cells in lupus remains largely
282 unknown. We show that type I IFN is one of the upstream signals that activate mTORC2 in T
283 cells. One of the downstream effects of type I IFN-mTORC2 activation is to promote CD69
284 expression and T cell lymphopenia. However, our data also showed that mTORC2 is only part of
285 type I IFN program that controls T cell egress, because RICTOR deficiency only modestly
286 prevented poly(I:C) induced lymphopenia. The prevailing theory on the pathogenesis of the
287 lymphopenia in lupus has been centered on antilymphocyte antibodies (46). Our study suggests
288 that elevated type I IFN production may be another contributing factor for the lymphopenia

289 phenotype in lupus. Consistent with this idea, recent clinical trial showed that type I IFN receptor
290 blockade can correct the T cell lymphopenia phenotype in patients with SLE (47).
291
292 It is worth noting that while RICTOR deficiency greatly reduced Tfh differentiation in Lpr mice,
293 it did not significantly affect Th1 and Th17 subsets, T cell IL-2 production and T cell
294 proliferation. These observations are consistent with our hypothesis that mTORC2 specifically
295 promotes Tfh differentiation without substantial effects on T cell activation, proliferation and
296 other effector T cell lineages. This is in contrast to mTORC1, which is required for T cell
297 quiescence exit and all effector T cell lineages (22). Thus, our data suggest that targeting
298 mTORC2 may specifically suppress Tfh lineage, which may have relatively smaller
299 immunosuppressive side effects, compared to inhibition of mTORC1. Altogether, our results
300 support the notion that mTORC2 is a novel target for lupus treatment, which warrants further
301 exploration in preclinical and, potentially, clinical studies.
302

303 **MATERIAL and METHODS**
304 **Mice**

305 *Cd4*^{Cre}*Rictor*$^{fl/fl}$ and *OX40*^{Cre}*Rictor*$^{fl/fl}$ mice have been described before (23). C57BL/6-*Fas*^{Lpr}
306 mice were purchased from The Jackson Laboratory. Mice were bred and maintained under
307 specific pathogen-free conditions in Department of Comparative Medicine of Mayo Clinic with
308 IACUC approval.

309 **ELISA**

310 For autoantibodies detection in sera, 96-well plates (2596; Costar) were coated with ssDNA and
311 chromatin (Sigma-Aldrich) in PBS overnight at 4C° used at a concentration of 1.6 μg/ml and 5
312 μg/ml, respectively. Plates were washed twice (0.05% Tween 20 in PBS), blocked with 5%

313 blocking protein (Bio-Rad) for 1 h, and washed twice, and serially diluted sera samples were
314 added for 1.5 h at 37 °C. Plates were washed four times and horseradish peroxidase (HRP)-
315 conjugated detection Abs for IgG (Bethyl Laboratories) were added for 1 h at RT, washed four
316 times, and tetramethylbenzidine (TMB) substrate was added. Reaction was stopped using 2N
317 H_2SO_4 and read at 450 nm. Mouse total IgM, IgG, IgG2b and IgG3 in sera were measured with
318 the kits from Invitrogen.

319 **Immunofluorescence staining**

320 Kidneys were obtained from 6-month-old B6, Lpr and Lpr. *Rictor*$^{fl/fl}$ mice, and fixed in 4%
321 paraformaldehyde (PFA) overnight, osmotically dehydrated in 20 % (w/v) sucrose, embedded in
322 OCT, and cryosectioned to 6 μM. Sections were fixed in −20°C acetone for 2 min and blocked in
323 PBS containing 8% goat serum, 1% bovine serum albumin (BSA) and 0.1% Tween 20 for 45
324 min. Deposition of immunoglobulin (IgG) and complement component 3 (C3) in the kidney
325 tissue were stained with PE labeled goat anti-mouse IgG (Invitrogen) and FITC labeled rat anti-
326 mouse C3 (Cedarlane) antibodies. Similarly, spleens were obtained from 6 months old mice, and
327 processed as above. Frozen sections were fixed and blocked as described above, and incubated
328 with primary antibodies Biotin Peanut Agglutinin (PNA) (Vectorlabs), purified rat anti-mouse
329 CD3 (Biolegend) and PE labeled anti-mouse IgD (BD), or stained with Biotin anti-mouse CD138
330 (Biolegend) and PE labeled anti-mouse IgD at 4°C for 4 hours. Slides were then washed before
331 streptavidin-Alexa Fluor 488 conjugate (ThermoFisher) and Alexa Fluor 647 labeled goat anti-
332 rat secondary antibody (ThermoFisher) were added for 1 h at room temperature. Sections were
333 covered with coverslip and visualized under an Olympus BX51 fluorescence microscope.

334 **Flow cytometry**

335 Single-cell suspension was prepared by passing spleen and peripheral lymph nodes through a 70-
336 μm nylon mesh. For analysis of surface markers, cells were stained in PBS containing 1% (w/v)
337 BSA on ice for 30 min, with APC-labeled anti-ICOS (clone: 7E.17G9; BD), PE-Cy7-labeled anti
338 PD-1 (clone: RMPI-30; BioLegend), Super Bright 600–labeled anti-CD4 (Clone: SK-3;
339 eBioscience), BV510-labeld anti-CD8a (clone:53-6.7; BioLegend); APC-Cy7-labeled TCRβ
340 (clone: H57-597; BioLegend), APC anti-CD162 (PSGL1; clone: 2PH1; BD), BV605-labeled
341 anti-CD25 (clone: PC61; BioLegend), PE-Cy7–labeled anti-CD19 (clone: 6D5; BioLegend),
342 BV605-labeled B220 (clone: RA3-6B2; BioLegend), PE-labeled anti-Fas (clone: Jo2; BD),
343 BV785-labeled anti-CD138 (clone: 281-2; BioLegend), APC-labeled anti-IgD (clone: IA6-2;
344 BioLegend), PerCP-Cyanine5.5-labeled anti-CD38 (clone: 90; BioLegend), FITC-labeled anti-
345 IgG1 (clone: RMG1-1; BioLegend), APC-labeled anti-IL7Rα (clone: SB/199; BioLegend),
346 FITC-labeled anti-CD69 (clone: H1.2F3; Tonbo Bio), PE-labeled anti-CD153 (clone: RM153;
347 eBioscience), PE-labeled anti-CD73 (clone: TY/11.8; BioLegend) and APC-labeled anti-FR4
348 (clone: 12A5; BD). Cell viability was assessed using the Fixable Dye Ghost 540 (Tonbo
349 Bioscience), or 7AAD. CXCR5 and PNA were stained with biotinylated anti-CXCR5 (clone:
350 2G8, BD Biosciences) or biotinylated peanut agglutinin (FL10-71; Vectorlabs), followed by
351 staining with streptavidin-conjugated PE (BD Biosciences). Splenocytes and peripheral lymph
352 node cells were cultured for 4 h at 37°C in complete medium (1640 RPMI + 10% FBS)
353 containing ionomycin (1 μg/ml), PMA (50 ng/ml) and Monensin solution (1,000×; BioLegend)
354 for cytokines detection. Intracellular cytokine staining of IFN-γ (clone: XMG1.2; eBioscience),
355 IL-2 (clone: JES6-5H4; BioLegend) and IL-17A (clone: TC11-18H10.1; BioLegend) were
356 performed using the BD Cytofix/Cytoperm and Perm/Wash buffers or, for transcriptional factors
357 FoxP3 (clone: FJK-16s; eBioscience), Bcl6 (clone: K112-91, BD) and Ki67 (clone: SolA15;

358 eBioscience) staining using the eBioscience Transcription Factor Staining Buffer Set. Phosflow
359 staining for AF647 conjugated phosphor-AKT (S473) (D9E; Cell signaling) was performed
360 using Phosflow Fix/Perm kit (BD Biosciences). Flow cytometry was performed on the Attune
361 NxT (ThermoFisher) cytometer, and analysis was performed using FlowJo software (Tree Star).

362 **Immunoblotting**

363 For immunoblotting, cells were lysed in lysis buffer with protease and phosphatase inhibitors
364 (Sigma-Aldrich). Protein concentration in samples was quantified by BCA assay (Thermo Fisher
365 Scientific) before loading the samples for electrophoresis and membrane transfer. The transferred
366 membrane was blocked with TBST (0.1% Tween 20) containing 5% BSA for 1 h at room
367 temperature. The membrane was incubated with primary antibodies overnight including anti-
368 phospho-AKT (Ser473) (clone: D9E; Cell Signaling), phospho-STAT1 (Tyr701) (clone: D4A7;
369 Cell Signaling), phospho-STAT2 (Tyr690) (Cell Signaling), phospho-S6 (Ser235/236) (clone:
370 D57.2.2E; Cell Signaling) and anti-β-actin (clone: 13E5; Sigma-Aldrich). Then, the membrane
371 was washed and incubated with the corresponding secondary antibody for subsequent enhanced
372 chemiluminescence (ECL; Thermo Fisher) exposure. The band intensity of all the immunoblot
373 was analyzed by ImageJ software.

374 **ICOS stimulation**

375 Cell isolation and flow cytometry of lymphocytes were as described. One million $CD4^+$ T cells
376 were activated with plate coated anti-CD3 and anti-CD28 (Bio X Cell). After 2 days activation,
377 T cells were removed from stimulation and rested overnight. Live cells were purified using
378 lymphocyte isolation buffer (MP Biomedicals), followed by stimulation with plate bound anti-
379 CD3 (2 µg/ml) and anti-ICOS (5 µg/ml; C398.4A; Biolegend) for 24 hours.

380 **Metabolic assay**

381 The bioenergetic activities of the OCR and ECAR were measured using a Seahorse XFe96
382 Extracellular Flux Analyzed following established protocols (Agilent). Briefly, equal number of
383 live $CD4^+$ T cells were seeded at 200,000 cells/well on Cell-Tak (Corning) coated XFe96 plate
384 with fresh XF media (Seahorse XF RPMI medium containing 10 mM glucose, 2 mM L-
385 glutamine, and 1 mM sodium pyruvate, PH 7.4; all reagents from Agilent). Basal OCR and
386 ECAR were measured in the presence of Oligomycin (1.5 μM; Sigma-Aldrich), FCCP (1.5 μM;
387 Sigma-Aldrich), and Rotenone (1 μM; Sigma-Aldrich)/ Antimycin A (1 μM; Sigma-Aldrich) in
388 Mito Stress assay. For ECAR measurement in ICOS secondary stimulated $CD4^+$ T cells,
389 glycolytic rate assay was performed according to the manufacturer's manual (Agilent) in
390 presence of Rotenone/Antimycin A and 2-DG (50 mM, Sigma-Aldrich)

391 **Poly(I:C) treatment and cell counting in peripheral blood**

392 *Cd4*^{Cre}*Rictor*$^{fl/fl}$ and wildtype mice were given intraperitoneal injection 200 μg poly(I:C) (Sigma-
393 Aldrich) in 200 μL PBS, and blood lymphocyte counts were assessed 16 and 40 hours later.
394 Briefly, to determine absolute blood cell counts, 50 μL peripheral blood with 5 μL EDTA was
395 collected, lysed with 1 mL ACK lysing buffer (ThermoFisher), and washed with PBS. Samples
396 were stained with anti-mouse CD19, CD4, CD8 and CD69 antibodies, washed with PBS once,
397 suspended with 500 μL PBS and loaded to Attune NxT cytometer with the acquisition of 250 μL
398 samples. Cell counts were calculated per 5 μL blood.

399 **Statistical Analysis**

400 Statistical analysis was performed using GraphPad Prism (version 8). P values were calculated
401 with Student's *t* test, or one-way ANOVA. $P < 0.05$ was considered significant.

402

403 **ACKNOWLEDGEMENTS**

404 We thank Drs. Virginia Shapiro and Jie Sun for thoughtful discussions. This work was partly
405 supported by Mayo Foundation for Medical Education and Research, and Center for Biomedical
406 Discovery at Mayo Clinic, and Lupus Research Alliance (696599, to H.Z.).

407

408 **REFERENCE**

409 1. Muskardin, T. L. W., and T. B. Niewold. 2018. Type I interferon in rheumatic diseases.
410 *Nat Rev Rheumatol* 14: 214-228.
411 2. Banchereau, J., and V. Pascual. 2006. Type I interferon in systemic lupus erythematosus
412 and other autoimmune diseases. *Immunity* 25: 383-392.
413 3. Morand, E. F., R. Furie, Y. Tanaka, I. N. Bruce, A. D. Askanase, C. Richez, S. C. Bae, P.
414 Z. Brohawn, L. Pineda, A. Berglind, R. Tummala, and T.-T. Investigators. 2020. Trial of
415 Anifrolumab in Active Systemic Lupus Erythematosus. *The New England journal of medicine*
416 382: 211-221.
417 4. Klarquist, J., R. Cantrell, M. A. Lehn, K. Lampe, C. M. Hennies, K. Hoebe, and E. M.
418 Janssen. 2020. Type I IFN Drives Experimental Systemic Lupus Erythematosus by Distinct
419 Mechanisms in CD4 T Cells and B Cells. *Immunohorizons* 4: 140-152.
420 5. Liu, Z., R. Bethunaickan, W. Huang, U. Lodhi, I. Solano, M. P. Madaio, and A.
421 Davidson. 2011. Interferon-alpha accelerates murine systemic lupus erythematosus in a T cell-
422 dependent manner. *Arthritis Rheum* 63: 219-229.
423 6. Shiow, L. R., D. B. Rosen, N. Brdickova, Y. Xu, J. An, L. L. Lanier, J. G. Cyster, and M.
424 Matloubian. 2006. CD69 acts downstream of interferon-alpha/beta to inhibit S1P1 and
425 lymphocyte egress from lymphoid organs. *Nature* 440: 540-544.
426 7. Kamphuis, E., T. Junt, Z. Waibler, R. Forster, and U. Kalinke. 2006. Type I interferons
427 directly regulate lymphocyte recirculation and cause transient blood lymphopenia. *Blood* 108:
428 3253-3261.
429 8. Su, C. C., W. Y. Shau, C. R. Wang, C. Y. Chuang, and C. Y. Chen. 1997. CD69 to CD3
430 ratio of peripheral blood mononuclear cells as a marker to monitor systemic lupus erythematosus
431 disease activity. *Lupus* 6: 449-454.
432 9. Tsujimura, S., T. Adachi, K. Saito, and Y. Tanaka. 2017. Role of P-glycoprotein on
433 CD69(+)CD4(+) cells in the pathogenesis of proliferative lupus nephritis and non-responsiveness
434 to immunosuppressive therapy. *RMD Open* 3: e000423.
435 10. Oke, V., I. Gunnarsson, J. Dorschner, S. Eketjall, A. Zickert, T. B. Niewold, and E.
436 Svenungsson. 2019. High levels of circulating interferons type I, type II and type III associate
437 with distinct clinical features of active systemic lupus erythematosus. *Arthritis Res Ther* 21: 107.
438 11. Liu, Z., and A. Davidson. 2012. Taming lupus-a new understanding of pathogenesis is
439 leading to clinical advances. *Nature medicine* 18: 871-882.
440 12. Mountz, J. D., H. C. Hsu, and A. Ballesteros-Tato. 2019. Dysregulation of T Follicular
441 Helper Cells in Lupus. *J Immunol* 202: 1649-1658.
442 13. Choi, J. Y., J. H. Ho, S. G. Pasoto, V. Bunin, S. T. Kim, S. Carrasco, E. F. Borba, C. R.
443 Goncalves, P. R. Costa, E. G. Kallas, E. Bonfa, and J. Craft. 2015. Circulating follicular helper-

like T cells in systemic lupus erythematosus: association with disease activity. *Arthritis Rheumatol* 67: 988-999.
14. Crotty, S. 2019. T Follicular Helper Cell Biology: A Decade of Discovery and Diseases. *Immunity* 50: 1132-1148.
15. Odegard, J. M., B. R. Marks, L. D. DiPlacido, A. C. Poholek, D. H. Kono, C. Dong, R. A. Flavell, and J. Craft. 2008. ICOS-dependent extrafollicular helper T cells elicit IgG production via IL-21 in systemic autoimmunity. *J Exp Med* 205: 2873-2886.
16. Poholek, A. C., K. Hansen, S. G. Hernandez, D. Eto, A. Chandele, J. S. Weinstein, X. Dong, J. M. Odegard, S. M. Kaech, A. L. Dent, S. Crotty, and J. Craft. 2010. In vivo regulation of Bcl6 and T follicular helper cell development. *J Immunol* 185: 313-326.
17. Lee, S. K., R. J. Rigby, D. Zotos, L. M. Tsai, S. Kawamoto, J. L. Marshall, R. R. Ramiscal, T. D. Chan, D. Gatto, R. Brink, D. Yu, S. Fagarasan, D. M. Tarlinton, A. F. Cunningham, and C. G. Vinuesa. 2011. B cell priming for extrafollicular antibody responses requires Bcl-6 expression by T cells. *J Exp Med* 208: 1377-1388.
18. Jenks, S. A., K. S. Cashman, M. C. Woodruff, F. E. Lee, and I. Sanz. 2019. Extrafollicular responses in humans and SLE. *Immunol Rev* 288: 136-148.
19. Mizui, M., and G. C. Tsokos. 2018. Targeting Regulatory T Cells to Treat Patients With Systemic Lupus Erythematosus. *Front Immunol* 9: 786.
20. Costa, N., O. Marques, S. I. Godinho, C. Carvalho, B. Leal, A. M. Figueiredo, C. Vasconcelos, A. Marinho, M. F. Moraes-Fontes, A. Gomes da Costa, C. Ponte, R. Campanilho-Marques, T. Coias, A. R. Martins, J. F. Viana, M. Lima, B. Martins, and C. Fesel. 2017. Two separate effects contribute to regulatory T cell defect in systemic lupus erythematosus patients and their unaffected relatives. *Clin Exp Immunol* 189: 318-330.
21. Saxton, R. A., and D. M. Sabatini. 2017. mTOR Signaling in Growth, Metabolism, and Disease. *Cell* 169: 361-371.
22. Zeng, H., and H. Chi. 2017. mTOR signaling in the differentiation and function of regulatory and effector T cells. *Curr Opin Immunol* 46: 103-111.
23. Zeng, H., S. Cohen, C. Guy, S. Shrestha, G. Neale, S. A. Brown, C. Cloer, R. J. Kishton, X. Gao, B. Youngblood, M. Do, M. O. Li, J. W. Locasale, J. C. Rathmell, and H. Chi. 2016. mTORC1 and mTORC2 Kinase Signaling and Glucose Metabolism Drive Follicular Helper T Cell Differentiation. *Immunity* 45: 540-554.
24. Zeng, H., K. Yang, C. Cloer, G. Neale, P. Vogel, and H. Chi. 2013. mTORC1 couples immune signals and metabolic programming to establish T(reg)-cell function. *Nature* 499: 485-490.
25. Shi, H., N. M. Chapman, J. Wen, C. Guy, L. Long, Y. Dhungana, S. Rankin, S. Pelletier, P. Vogel, H. Wang, J. Peng, K. L. Guan, and H. Chi. 2019. Amino Acids License Kinase mTORC1 Activity and Treg Cell Function via Small G Proteins Rag and Rheb. *Immunity* 51: 1012-1027 e1017.
26. Chapman, N. M., H. Zeng, T. M. Nguyen, Y. Wang, P. Vogel, Y. Dhungana, X. Liu, G. Neale, J. W. Locasale, and H. Chi. 2018. mTOR coordinates transcriptional programs and mitochondrial metabolism of activated Treg subsets to protect tissue homeostasis. *Nat Commun* 9: 2095.
27. Hosokawa, T., T. Kimura, S. Nada, T. Okuno, D. Ito, S. Kang, S. Nojima, K. Yamashita, T. Nakatani, Y. Hayama, Y. Kato, Y. Kinehara, M. Nishide, N. Mikami, S. Koyama, H. Takamatsu, D. Okuzaki, N. Ohkura, S. Sakaguchi, M. Okada, and A. Kumanogoh. 2017.

489 Lamtor1 Is Critically Required for CD4(+) T Cell Proliferation and Regulatory T Cell
490 Suppressive Function. *J Immunol* 199: 2008-2019.
491 28. Shrestha, S., K. Yang, C. Guy, P. Vogel, G. Neale, and H. Chi. 2015. Treg cells require
492 the phosphatase PTEN to restrain TH1 and TFH cell responses. *Nat Immunol* 16: 178-187.
493 29. Huynh, A., M. DuPage, B. Priyadharshini, P. T. Sage, J. Quiros, C. M. Borges, N.
494 Townamchai, V. A. Gerriets, J. C. Rathmell, A. H. Sharpe, J. A. Bluestone, and L. A. Turka.
495 2015. Control of PI(3) kinase in Treg cells maintains homeostasis and lineage stability. *Nat*
496 *Immunol* 16: 188-196.
497 30. Charbonnier, L. M., Y. Cui, E. Stephen-Victor, H. Harb, D. Lopez, J. J. Bleesing, M. I.
498 Garcia-Lloret, K. Chen, A. Ozen, P. Carmeliet, M. O. Li, M. Pellegrini, and T. A. Chatila. 2019.
499 Functional reprogramming of regulatory T cells in the absence of Foxp3. *Nat Immunol* 20: 1208-
500 1219.
501 31. Wyman, B., and A. Perl. 2020. Metabolic pathways mediate pathogenesis and offer
502 targets for treatment in rheumatic diseases. *Curr Opin Rheumatol* 32: 184-191.
503 32. Kato, H., and A. Perl. 2014. Mechanistic target of rapamycin complex 1 expands Th17
504 and IL-4+ CD4-CD8- double-negative T cells and contracts regulatory T cells in systemic lupus
505 erythematosus. *J Immunol* 192: 4134-4144.
506 33. Kato, H., and A. Perl. 2018. Blockade of Treg Cell Differentiation and Function by the
507 Interleukin-21-Mechanistic Target of Rapamycin Axis Via Suppression of Autophagy in Patients
508 With Systemic Lupus Erythematosus. *Arthritis Rheumatol* 70: 427-438.
509 34. Li, W., A. A. Titov, and L. Morel. 2017. An update on lupus animal models. *Curr Opin*
510 *Rheumatol* 29: 434-441.
511 35. Braun, D., P. Geraldes, and J. Demengeot. 2003. Type I Interferon controls the onset and
512 severity of autoimmune manifestations in lpr mice. *Journal of autoimmunity* 20: 15-25.
513 36. Nickerson, K. M., J. L. Cullen, M. Kashgarian, and M. J. Shlomchik. 2013. Exacerbated
514 autoimmunity in the absence of TLR9 in MRL.Fas(lpr) mice depends on Ifnar1. *J Immunol* 190:
515 3889-3894.
516 37. Lee, K., P. Gudapati, S. Dragovic, C. Spencer, S. Joyce, N. Killeen, M. A. Magnuson,
517 and M. Boothby. 2010. Mammalian target of rapamycin protein complex 2 regulates
518 differentiation of Th1 and Th2 cell subsets via distinct signaling pathways. *Immunity* 32: 743-
519 753.
520 38. Delgoffe, G. M., K. N. Pollizzi, A. T. Waickman, E. Heikamp, D. J. Meyers, M. R.
521 Horton, B. Xiao, P. F. Worley, and J. D. Powell. 2011. The kinase mTOR regulates the
522 differentiation of helper T cells through the selective activation of signaling by mTORC1 and
523 mTORC2. *Nat Immunol* 12: 295-303.
524 39. Kelley, V. E., and J. B. Roths. 1985. Interaction of mutant lpr gene with background
525 strain influences renal disease. *Clin Immunol Immunopathol* 37: 220-229.
526 40. Chen, L., L. Diao, Y. Yang, X. Yi, B. L. Rodriguez, Y. Li, P. A. Villalobos, T. Cascone,
527 X. Liu, L. Tan, P. L. Lorenzi, A. Huang, Q. Zhao, D. Peng, J. J. Fradette, D. H. Peng, C.
528 Ungewiss, J. Roybal, P. Tong, J. Oba, F. Skoulidis, W. Peng, B. W. Carter, C. M. Gay, Y. Fan,
529 C. A. Class, J. Zhu, J. Rodriguez-Canales, M. Kawakami, L. A. Byers, S. E. Woodman, V. A.
530 Papadimitrakopoulou, E. Dmitrovsky, J. Wang, S. E. Ullrich, Wistuba, II, J. V. Heymach, F. X.
531 Qin, and D. L. Gibbons. 2018. CD38-Mediated Immunosuppression as a Mechanism of Tumor
532 Cell Escape from PD-1/PD-L1 Blockade. *Cancer Discov* 8: 1156-1175.
533 41. MacLennan, I. C., K. M. Toellner, A. F. Cunningham, K. Serre, D. M. Sze, E. Zuniga, M.
534 C. Cook, and C. G. Vinuesa. 2003. Extrafollicular antibody responses. *Immunol. Rev.* 194: 8-18.

535 42. Clement, R. L., J. Daccache, M. T. Mohammed, A. Diallo, B. R. Blazar, V. K. Kuchroo,
536 S. B. Lovitch, A. H. Sharpe, and P. T. Sage. 2019. Follicular regulatory T cells control humoral
537 and allergic immunity by restraining early B cell responses. *Nat. Immunol.* 20: 1360-1371.
538 43. Morel, L. 2017. Immunometabolism in systemic lupus erythematosus. *Nat Rev*
539 *Rheumatol* 13: 280-290.
540 44. Yin, Y., S. C. Choi, Z. Xu, L. Zeumer, N. Kanda, B. P. Croker, and L. Morel. 2016.
541 Glucose Oxidation Is Critical for CD4+ T Cell Activation in a Mouse Model of Systemic Lupus
542 Erythematosus. *J Immunol* 196: 80-90.
543 45. Yin, Y., S. C. Choi, Z. Xu, D. J. Perry, H. Seay, B. P. Croker, E. S. Sobel, T. M. Brusko,
544 and L. Morel. 2015. Normalization of CD4+ T cell metabolism reverses lupus. *Sci Transl Med* 7:
545 274ra218.
546 46. Fayyaz, A., A. Igoe, B. T. Kurien, D. Danda, J. A. James, H. A. Stafford, and R. H.
547 Scofield. 2015. Haematological manifestations of lupus. *Lupus Sci Med* 2: e000078.
548 47. Casey, K. A., X. Guo, M. A. Smith, S. Wang, D. Sinibaldi, M. A. Sanjuan, L. Wang, G.
549 G. Illei, and W. I. White. 2018. Type I interferon receptor blockade with anifrolumab corrects
550 innate and adaptive immune perturbations of SLE. *Lupus Sci Med* 5: e000286.
551

552 **FIGURE LEGENDS**

553 **Figure 1. mTORC2 signaling in B6, Lpr and Lpr.*Rictor*$^{-/-}$ T cells.** (A) Immunoblot analysis
554 of p-AKT$_{473}$ in B6 and Lpr CD4^{+} T cells isolated from peripheral lymph nodes (pLN). Right,
555 summary of the relative p-AKT$_{473}$ expression (normalized to that in B6 CD4^{+} T cells). (B)
556 Immunoblot analysis of p-AKT$_{473}$, p-STAT1, and p-STAT2 in CD4^{+} T cells from B6 and
557 CD4^{cre}*Rictor*$^{fl/fl}$ mice stimulated with or without anti-CD3/anti-CD28 in the presence or absence
558 of IFNα for 1 and 6 hours. Right, summaries of the relative p-AKT$_{473}$ expression (normalized to
559 that in B6 CD4^{+} T cells without any stimulation) for 1 and 6 hours, respectively. (C) Flow
560 cytometry analysis of p-AKT$_{473}$ expression in CD4^{+} T cells treated with IFNα alone, or in
561 combination with anti-CD3/anti-CD28 overnight. Right, summary of the relative pAKT473
562 expression (normalized to that in B6 CD4^{+} T cells without any stimulation). (D) and (E) B6 and
563 CD4^{cre}*Rictor*$^{fl/fl}$ mice were administered with poly(I:C) intraperitoneally. (D) Expression of
564 CD69 in blood CD4^{+} T cells from B6 and CD4^{cre}*Rictor*$^{fl/fl}$ mice after poly(I:C) administration.
565 Numbers indicate the percentages of CD69^{+} cells. Right, summary of CD69^{+} percentage in CD4^{+}
566 T cells at baseline or treated with poly(I:C) for 16 h and 40 h. (E) Blood CD4^{+} T cell counts were
567 determined before and after poly(I:C) treatment. (F) Expression of CD69 in CD4^{+} T cells from
568 B6, Lpr and Lpr.*Rictor*$^{-/-}$ mice. Right, summary of CD69^{+} percentages among pLN CD4^{+} T
569 cells. (G) Blood CD4^{+} T cell counts were determined in 4-6 months old B6, Lpr and Lpr.*Rictor*$^{-/-}$
570 mice. NS, not significant; * $P < 0.05$, ** $P < 0.01$, *** $P < 0.001$, **** $P < 0.0001$ (A-E,
571 unpaired Student's *t* test, F and G, one-way ANOVA). Results were presentative of 4 (A, B), or
572 pooled from at least 3 (A-G) independent experiments. Error bars represent SEM.

573

574 **Figure 2. Rictor deletion in T cells rectifies immunopathology in Lpr mice.** Images of
575 spleens (A) and peripheral lymph nodes (B) taken from 6 months old B6, Lpr and Lpr.*Rictor*$^{-/-}$
576 mice. Right, summary of spleen weight, total cellularity of spleen (A) and lymph nodes (B). (C)
577 Titers of total immunoglobulin (Ig) M, IgG, IgG2b and IgG3 were measured by ELISA. (D)
578 Titers of anti-ssDNA (left) and anti-chromatin (right) were measured by ELISA. Samples were
579 from 9 months old B6, Lpr and Lpr.*Rictor*$^{-/-}$ mice. (E) Expression of B220 and TCRβ on
580 lymphocytes. Right, the frequencies (upper panels) and absolute numbers (lower panels) of
581 B220^{+}TCRβ^{+}, B220^{-}TCRβ^{+}, B220^{+}TCRβ^{-} cells. (F) Flow cytometry analysis of CD4 and CD8 T
582 cells among B220^{-}TCRβ^{+} cells. Right, the frequency (left) and absolute number (right) of CD4^{-}
583 CD8^{-} T cell population. (E) and (F) Cells were from peripheral lymph nodes (pLN) of 6 months
584 old B6, Lpr and Lpr.*Rictor*$^{-/-}$ mice. NS, not significant; * $P < 0.05$, ** $P < 0.01$, *** $P < 0.001$,
585 **** $P < 0.0001$. *p* values were calculated with one-way ANOVA. Results (A-F) were pooled
586 from at least 3 independent experiments. Error bars represent SEM.
587
588 **Figure 3. mTORC2 in T cells is required for B cell hyper-activation in Lpr mice.** (A)
589 Immunofluorescence staining of peanut agglutinin (PNA), CD3 and IgD on spleen sections from
590 6 months old B6, Lpr and Lpr.*Rictor*$^{-/-}$ mice. (B) Flow cytometry analysis of GL-7 and IgD
591 expression among B220^{+}TCRβ^{-} cells. Right, the frequency of IgD^{-}GL-7^{+} germinal center (GC)
592 B cells. (C) Immunofluorescence staining of CD138 and IgD on spleen sections from 6 months
593 old B6, Lpr and Lpr.*Rictor*$^{-/-}$ mice. (D) Flow cytometry analysis of B220^{+}CD138^{int} and
594 B220^{lo}CD138^{hi} two populations. Right, the frequencies of B220^{+}CD138^{int} (left) and
595 B220^{lo}CD138^{hi} (right) among total lymphocytes. (B) and (D) Cells were from pLNs of 6 months
596 old B6, Lpr and Lpr.*Rictor*$^{-/-}$ mice. NS, not significant; *** $P < 0.001$, **** $P < 0.0001$ (one-

597 way ANOVA). Results were pooled from 3 (B and D) independent experiments. Error bars
598 represent SEM.
599
600 **Figure 4. Rictor deletion reduces Tfh differentiation and normalizes Treg homeostasis.** (A)
601 Expression of CXCR5 and BCL6 on B220^{-}CD4^{+} T cells. Right, the percentages of
602 BCL6^{+}CXCR5^{+} and BCL6^{-}CXCR5^{+} cells. (B) Expression of PSGL1 and CXCR5 on B220^{-}
603 CD4^{+} T cells. Right, the summary of PSGL1^{lo}CXCR5^{lo} extrafollicular (EF) Tfh cell percentages.
604 (C) Expression of ICOS and CXCR5 on B220^{-}CD4^{+} T cells. Right, the summary of ICOS^{+} cell
605 frequency. (D) Flow cytometry analysis of Treg cells (B220^{-}CD4^{+}Foxp3^{+}). Frequencies of
606 FOXP3^{+} cells in CD4^{+} T cells from spleen (left), peripheral lymph nodes (pLN) (middle) and
607 Peyer's patches (PP) (right). (E) The ratio between Tfh and Treg frequency (left) and the ratio
608 between Tfh and Tfr frequency (right) in CD4^{+} T cells from B6, Lpr and Lpr.*Rictor*$^{-/-}$ mice. (F)
609 Expression of IFNg and IL-17 in CD4^{+} T cells activated by PMA and ionomycin. Right,
610 frequencies of IFNg^{+} cells and IL-17^{+} cells. (G) Expression of IL-2 in CD4^{+} T cells activated by
611 PMA and ionomycin. Right, the frequency of IL-2^{+} cell. (H) Expression of Ki-67 in CD4^{+} T cells
612 from B6, Lpr and Lpr.*Rictor*$^{-/-}$ mice. Right, the summary of Ki-67^{+} cell frequency. (A-C, and E-
613 H) Cells were from pLNs of 6 months old B6, Lpr and Lpr.*Rictor*$^{-/-}$ mice. NS, not significant; *
614 $P < 0.05$, ** $P < 0.01$, *** $P < 0.001$, **** $P < 0.0001$ (one-way ANOVA). Results were pooled
615 from at least 3 (A-H) independent experiments. Error bars represent SEM.
616
617 **Figure 5. Metabolic activities in B6, Lpr and Lpr.*Rictor*$^{-/-}$ T cells.** (A) The basal respiration
618 and (B) basal extracellular acidification rate (ECAR) of CD4^{+} T from 2, 3, and 9 months old
619 mice cells under anti-CD3/anti-CD28 overnight activation, respectively. (C) The ECAR of CD4^{+}

620 T cells followed by sequential anti-CD3/anti-CD28, and anti-CD3/anti-ICOS stimulation
621 measured by glycolytic rate assay. Cells were from pLNs of 6 months old B6, Lpr and
622 Lpr.*Rictor*$^{-/-}$ mice. Right, summaries of basal glycolysis and compensatory glycolysis. Rot,
623 Rotenone; AA, Antimycin A; 2-DG, 2-deoxyglucose. NS, not significant; * $P < 0.05$, ** $P <$
624 0.01, *** $P < 0.001$, **** $P < 0.0001$ (one-way ANOVA). Results were presentative of 2 (A-B)
625 and 3 (C) independent experiments. Error bars represent SEM.
626
627
628

Figure 1

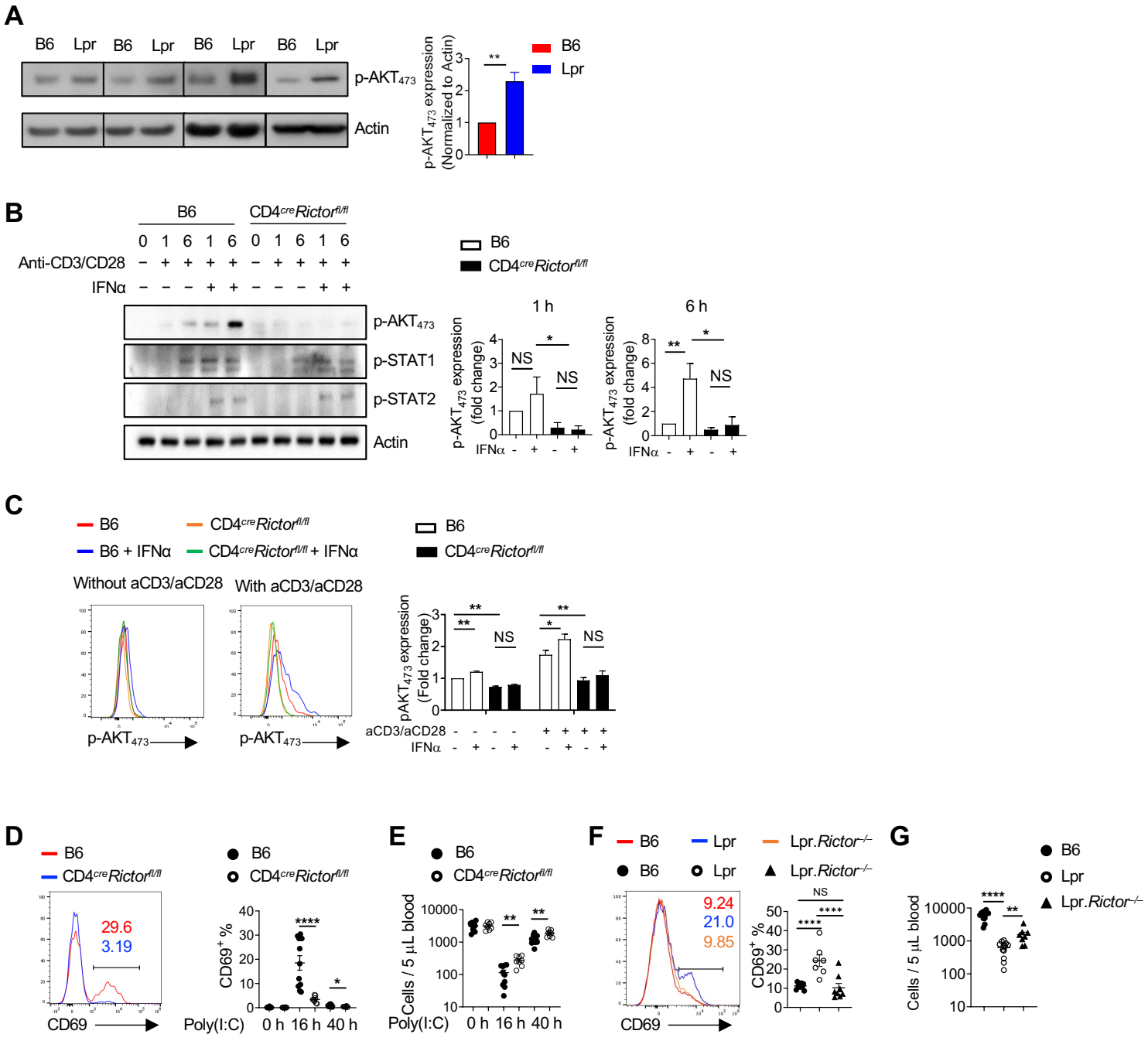
A
B6 Lpr B6 Lpr B6 Lpr B6 Lpr
p-AKT473
Actin
p-AKT473 expression (Normalized to Actin)
B6
Lpr
B
B6
CD4creRictorfl/fl
0 1 6 1 6 0 1 6 1 6
Anti-CD3/CD28
IFNα
p-AKT473
p-STAT1
p-STAT2
Actin
1 h
6 h
p-AKT473 expression (fold change)
NS
IFNα
C
B6
B6 + IFNα
CD4creRictorfl/fl
CD4creRictorfl/fl + IFNα
Without aCD3/aCD28
With aCD3/aCD28
p-AKT473
pAKT473 expression (Fold change)
aCD3/aCD28
D
29.6
3.19
CD69
CD69+ %
Poly(I:C)
0 h 16 h 40 h
E
Cells / 5 µL blood
F
9.24
21.0
9.85
Lpr.Rictor−/−
G

Figure 2

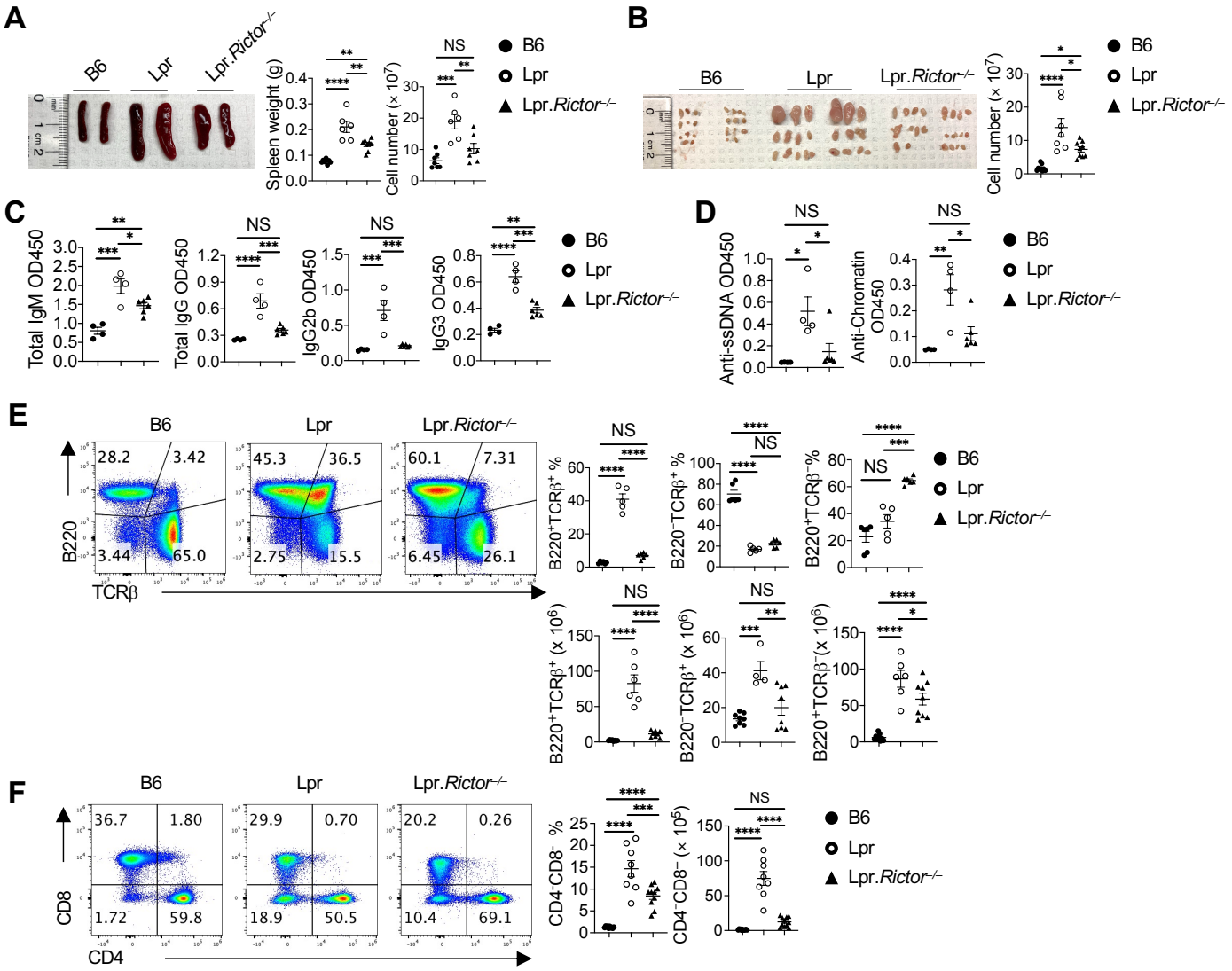
A
B6
Lpr
Lpr.Rictor-/-
Spleen weight (g)
Cell number (× 10^7)
NS
B6
Lpr
Lpr.Rictor-/-
B
B6
Lpr
Lpr.Rictor-/-
Cell number (× 10^7)
B6
Lpr
Lpr.Rictor-/-
C
Total IgM OD450
Total IgG OD450
IgG2b OD450
IgG3 OD450
NS
B6
Lpr
Lpr.Rictor-/-
D
Anti-ssDNA OD450
Anti-Chromatin OD450
NS
B6
Lpr
Lpr.Rictor-/-
E
B6
Lpr
Lpr.Rictor-/-
B220
TCRβ
28.2
3.42
3.44
65.0
45.3
36.5
2.75
15.5
60.1
7.31
6.45
26.1
B220+TCRβ+ %
B220-TCRβ+ %
B220+TCRβ- %
B220+TCRβ+ (x 10^6)
B220-TCRβ+ (x 10^6)
B220+TCRβ- (x 10^6)
NS
B6
Lpr
Lpr.Rictor-/-
F
B6
Lpr
Lpr.Rictor-/-
CD8
CD4
36.7
1.80
1.72
59.8
29.9
0.70
18.9
50.5
20.2
0.26
10.4
69.1
CD4-CD8- %
CD4-CD8- (x 10^5)
NS
B6
Lpr
Lpr.Rictor-/-

Figure 3

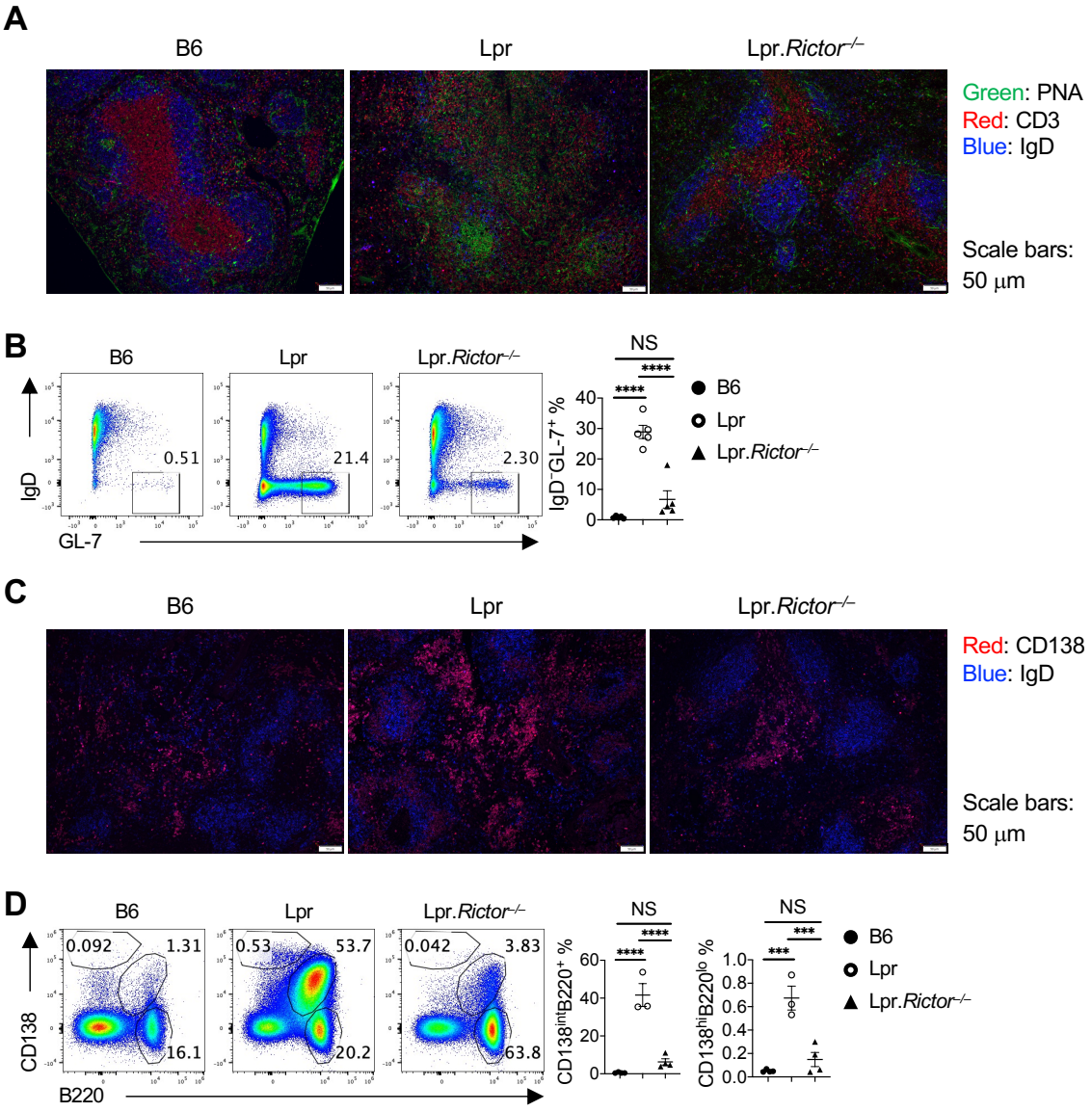
A
B6
Lpr
Lpr.Rictor-/-
Green: PNA
Red: CD3
Blue: IgD
Scale bars:
50 μm
B
B6
Lpr
Lpr.Rictor-/-
IgD
GL-7
0.51
21.4
2.30
NS
****
****
IgD-GL-7+ %
40
30
20
10
0
B6
Lpr
Lpr.Rictor-/-
C
B6
Lpr
Lpr.Rictor-/-
Red: CD138
Blue: IgD
Scale bars:
50 μm
D
B6
Lpr
Lpr.Rictor-/-
CD138
B220
0.092
1.31
16.1
0.53
53.7
20.2
0.042
3.83
63.8
NS
****
****
CD138intB220+ %
60
40
20
0
NS
***
***
CD138hiB220lo %
1.0
0.8
0.6
0.4
0.2
0.0
B6
Lpr
Lpr.Rictor-/-

Figure 4

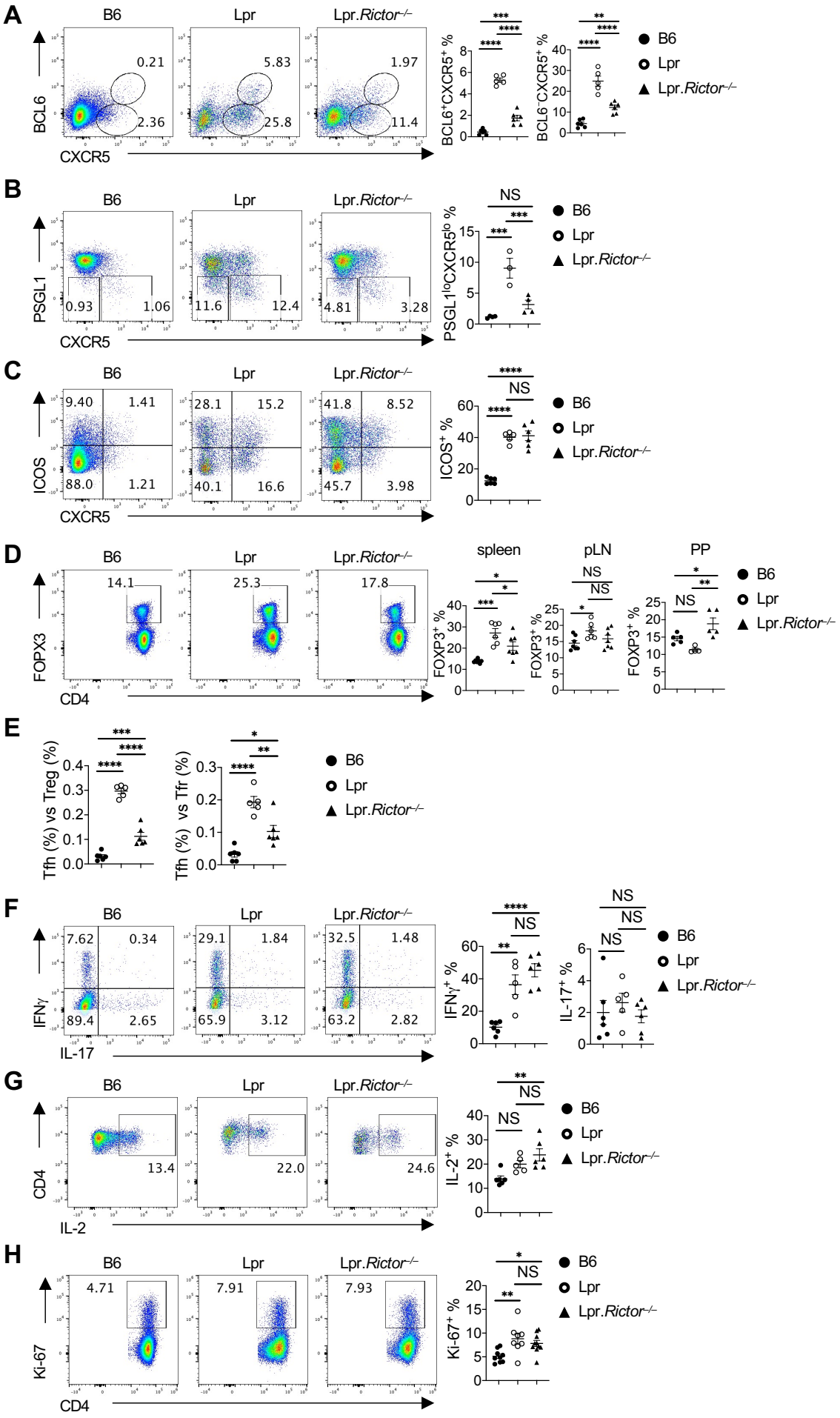
A
B6
Lpr
Lpr.Rictor-/-
BCL6
CXCR5
0.21
2.36
5.83
25.8
1.97
11.4
BCL6+CXCR5+ %
BCL6-CXCR5+ %
B6
Lpr
Lpr.Rictor-/-
B
PSGL1
0.93
1.06
11.6
12.4
4.81
3.28
PSGL1loCXCR5lo %
NS
C
ICOS
9.40
1.41
88.0
1.21
28.1
15.2
40.1
16.6
41.8
8.52
45.7
3.98
ICOS+ %
D
FOXP3
CD4
14.1
25.3
17.8
spleen
pLN
PP
FOXP3+ %
E
Tfh (%) vs Treg (%)
Tfh (%) vs Tfr (%)
F
IFNγ
IL-17
7.62
0.34
89.4
2.65
29.1
1.84
65.9
3.12
32.5
1.48
63.2
2.82
IFNγ+ %
IL-17+ %
G
CD4
IL-2
13.4
22.0
24.6
IL-2+ %
H
Ki-67
CD4
4.71
7.91
7.93
Ki-67+ %

Figure 5

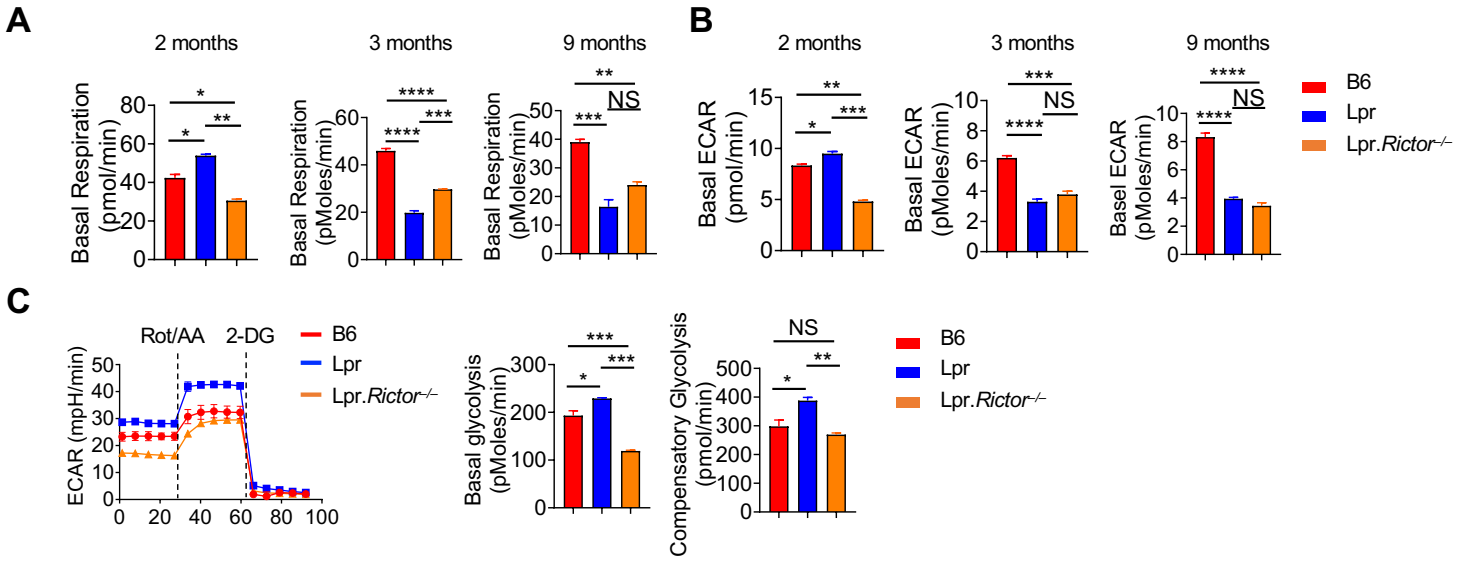
A
2 months
3 months
9 months
Basal Respiration (pmol/min)
Basal Respiration (pMoles/min)
Basal Respiration (pMoles/min)
B
Basal ECAR (pmol/min)
Basal ECAR (pMoles/min)
Basel ECAR (pMoles/min)
NS
B6
Lpr
Lpr.Rictor-/-
C
Rot/AA
2-DG
ECAR (mpH/min)
Basal glycolysis (pMoles/min)
Compensatory Glycolysis (pmol/min)

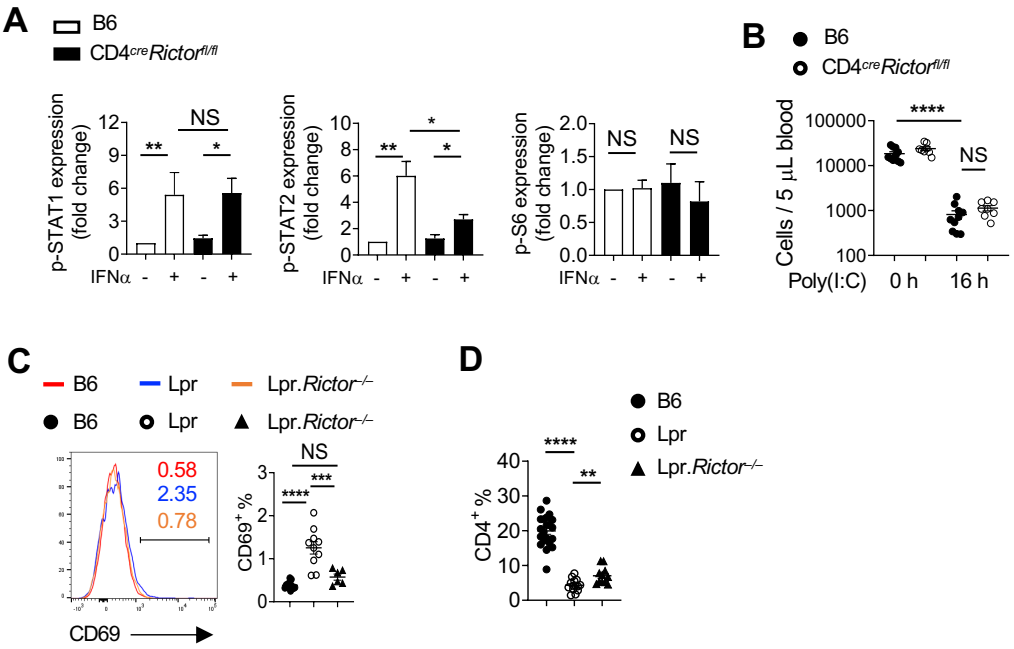

Supplemental Figure 1

(A) Immunoblot analysis of pSTAT1, pSTAT2 and p-S6 expression in CD4$^+$ T cells from B6 and CD4^{cre}*Rictor*$^{fl/fl}$ mice treated with or without IFNα in presence of anti-CD3/anti-CD28 for 6 hours. The relative expressions were normalized to them in B6 CD4$^+$ T cells without any stimulation. (B) Blood CD19$^+$ B cell counts were determined before and after poly(I:C) treatment in B6 and CD4^{cre}*Rictor*$^{fl/fl}$ mice. (C) Expression of CD69 was measured by flow cytometry in blood CD4$^+$ T cells from 4-6 months old B6, Lpr and Lpr.*Rictor*$^{-/-}$ mice. Right, summary of CD69$^+$ percentages among blood CD4$^+$ T cells. (D) Percentages of CD19$^-$CD4$^+$ T cells in blood from B6, Lpr and Lpr.*Rictor*–/– mice among total lymphocytes. NS, not significant; * $P < 0.05$, ** $P < 0.01$, *** $P < 0.001$, **** $P < 0.0001$ (A and B, unpaired Student's *t* test, C and D, one-way ANOVA). Results were pooled from at least 3 independent experiments. Error bars represent SEM.

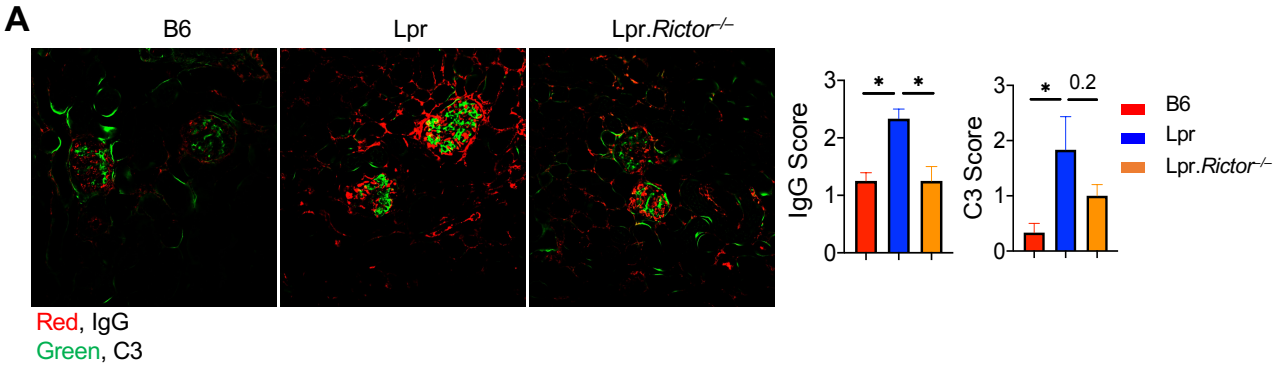

Supplemental Figure 2

(A) Immunofluorescence staining of IgG (Red) and C3 (Green) on 6 months old mice kidney sections. Right, the scores of IgG and C3 deposition. * $P < 0.05$ (one-way ANOVA). Results were pooled from 2 independent experiments. Error bars represent SEM.

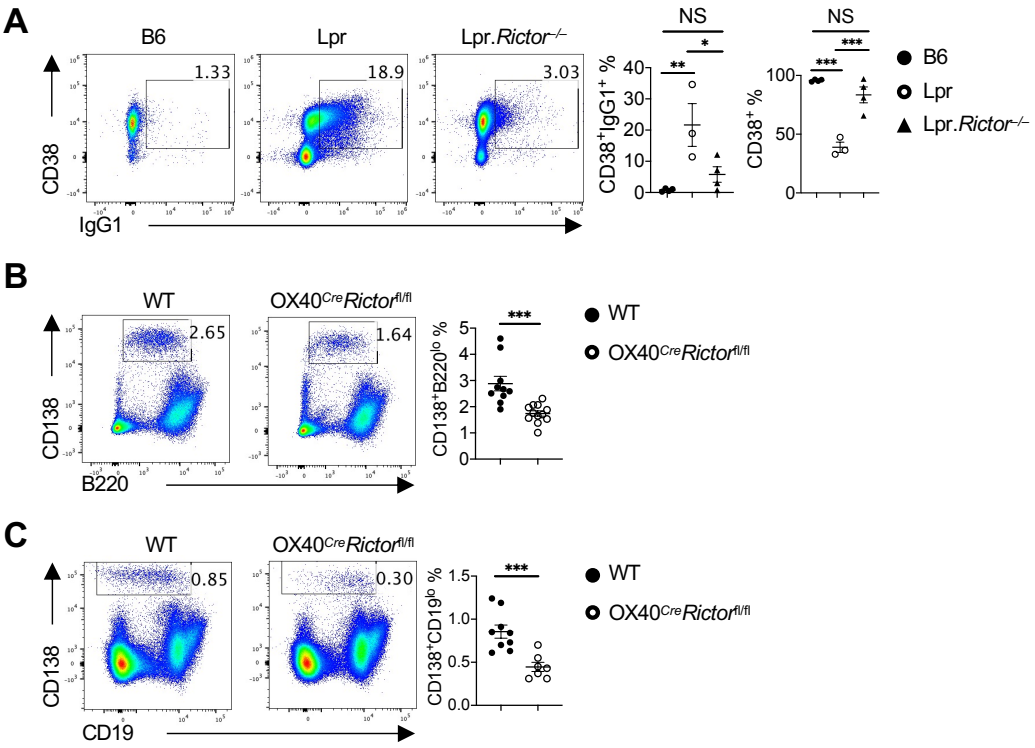

Supplemental Figure 3

(A) Expression of CD38 and IgG1 expression on B220^{+}TCRb^{-} B cells. Right, the frequencies of CD38^{+}IgG1^{+} B cells (left) and CD38^{+} percentages (right). (B-C) Flow cytometry analysis of CD138^{+}B220^{lo} or CD138^{+}CD19^{lo} plasmablasts from WT and OX40^{Cre}*Rictor*$^{fl/fl}$ mice after challenge with LCMV Armstrong strain (B) and immunization with NP-OVA. Right, the frequencies of plamablasts. NS, not significant; * $P < 0.05$, ** $P < 0.01$, *** $P < 0.001$, **** $P < 0.0001$ (A, one-way ANOVA, B and C, unpaired Student's *t* test). Results were pooled from 3 (A-B) or 2 (C) independent experiments. Error bars represent SEM.

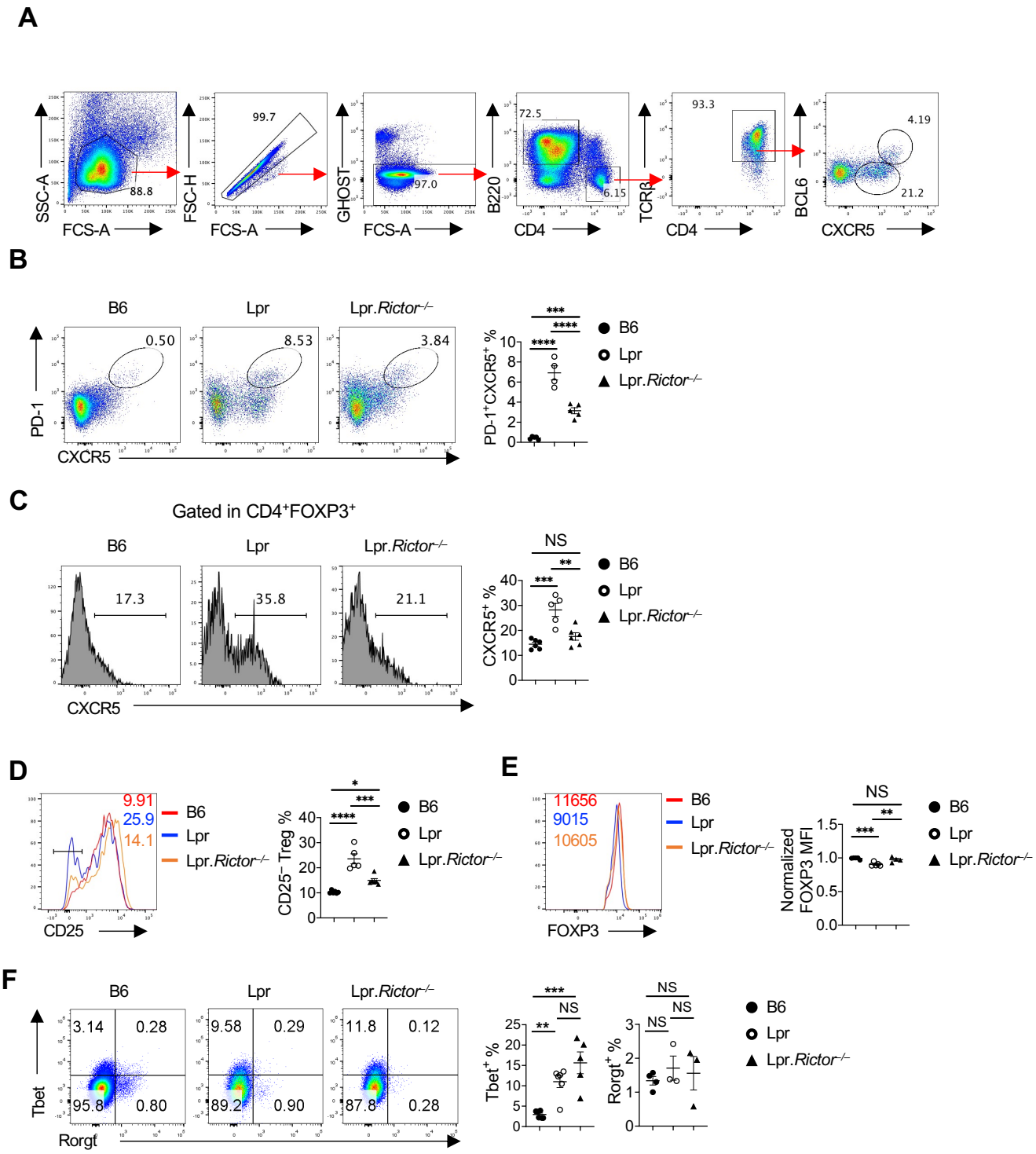

Supplemental Figure 4

(A) Gating strategy for analysis of Tfh cells.(B) Flow cytometry analysis of CXCR5 and PD-1 on B220^{-}CD4^{+} T cells. Right, the percentages of PD-1^{+}CXCR5^{+} cells. (C) Expression of CXCR5 in Tregs. Right, summary of CXCR5^{+} Tfr cell percentages. (D) Expression of CD25 on FOXP3^{+} Tregs. Numbers indicate the percentages of CD25^{-} Tregs. Right, summary of the percentages of CD25^{-} Tregs. (E) Expression of FOXP3 on FOXP3^{+} Tregs. Numbers indicate the MFI of FOXP3. Right, the summary of FOXP3 MFI. (F) Expression of Tbet and Rorgt on on B220^{-}CD4^{+} T cells. Right, summary of Tbet^{+} and Rorgt^{+} cell percentages. Cells were from peripheral lymph nodes (pLNs) of 6 months old B6, Lpr and Lpr.*Rictor*$^{-/-}$ mice. NS, not significant; ** $P < 0.01$, *** $P < 0.001$, **** $P < 0.0001$ (one-way ANOVA). Results were pooled from at least 3 independent experiments. Error bars represent SEM.

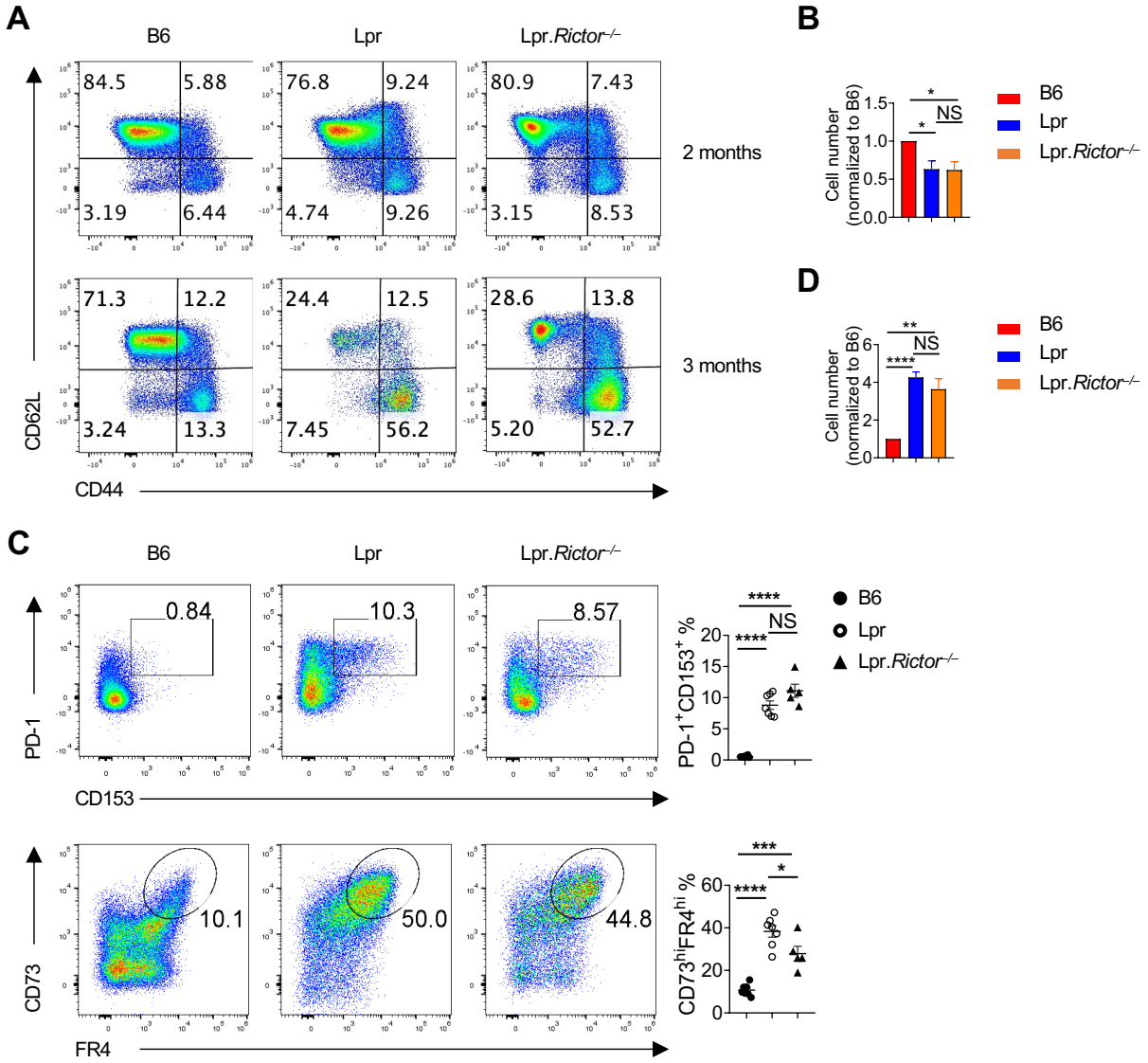

Supplemental Figure 5

(A) Flow cytometry analysis of CD44 vs. CD62L in B220^{-}CD4^{+} T cells among 2 and 3 months old B6, Lpr and Lpr.*Rictor*$^{-/-}$ mice, respectively. (B) Summary of cell numbers for B220^{-}CD4^{+} T cells with anti-CD3/anti-CD28 activation for 72 hours. Numbers were normalized to B6 control. (C) Flow cytometry analysis of PD-1 vs. CD153 and CD73 vs. FR4 expression in B220^{-}CD4^{+} T cells among 6 months old B6, Lpr and Lpr.*Rictor*$^{-/-}$ mice. Right, summaries of frequencies of PD-1^{+}CD153^{+} and CD73^{hi}FR4^{hi} populations. (D) Summary of cell numbers for B220^{-}CD4^{+} T cells activated with anti-CD3/anti-CD28, and then with secondary anti-CD3/ICOS stimulation. Numbers were normalized to B6 control. NS, not significant; * $P < 0.05$, ** $P < 0.01$, *** $P < 0.001$, **** $P < 0.0001$ (one-way ANOVA). Results were pooled from at least 3 independent experiments. Error bars represent SEM.